PHYSICS OF FLUIDS **28**, 024110 (2016)

Stabilization of the hypersonic boundary layer by finite-amplitude streaks

Jie Ren,[1,a)] Song Fu,[1,b)] and Ardeshir Hanifi[2,c)]
[1]*School of Aerospace Engineering, Tsinghua University, Beijing 100084, China*
[2]*Department of Mechanics, Linné FLOW Centre, SeRC, KTH Royal Institute of Technology, SE-100 44 Stockholm, Sweden*

(Received 8 August 2015; accepted 2 February 2016; published online 19 February 2016)

Stabilization of two-dimensional disturbances in hypersonic boundary layer flows by finite-amplitude streaks is investigated using nonlinear parabolized stability equations. The boundary-layer flows at Mach numbers 4.5 and 6.0 are studied in which both first and second modes are supported. The streaks considered here are driven either by the so-called optimal perturbations (Klebanoff-type) or the centrifugal instability (Görtler-type). When the streak amplitude is in an appropriate range, i.e., large enough to modulate the laminar boundary layer but low enough to not trigger secondary instability, both first and second modes can effectively be suppressed. © *2016 AIP Publishing LLC.* [http://dx.doi.org/10.1063/1.4941989]

I. INTRODUCTION

Recent studies on finite-amplitude streaks have provided a promising control methodology to attenuate the Tollmien-Schlichting (T-S) waves thereby delaying or even suppressing flow transition.[1] Analysis on this passive control strategy is now extended to high-speed flows in the current study.

Streaky structures inside the boundary layers are often observed in a number of practical situations, triggered either naturally or artificially, e.g., flows in the presence of high free-stream turbulence (FST),[2] over surfaces with concave curvature (Görtler instability)[3] or tripped by roughness elements of certain geometries.[4] Laminar-turbulent transition in flows dominated by streamwise-elongated streaks is often caused by their sinuous/varicose secondary instabilities.[5] Prior to the onset of secondary instabilities,[6] T-S waves can, to a remarkable extent, be stabilized. The direct numerical simulations (DNSs) by Cossu and Brandt[7,8] showed that the T-S waves can be effectively stabilized by optimal streaks. Here, "optimal" stands for the disturbance which experience maximum energy growth measured in a prescribed spatial or temporal range. In the Blasius boundary layer, as investigated by Andersson *et al.*[9] and Luchini,[10] the *Re*-independent optimal parameters are spanwise wavenumber $\beta_{opt} = 0.45$ and frequency $\omega_{opt} = 0$. Increase in the amplitude of the streaks shows a stronger effect of stabilization. This is due to the modification to the mean flow caused by the nonlinear development of streaks. The optimal streaks, nevertheless, are not necessarily "optimal" for the stabilization of T-S waves.[11]

The experiments performed by Fransson and co-workers successfully materialized the idea of passive control with circular roughness elements[12–14] and miniature vortex generators (MVGs).[15–18] The threshold streak amplitude is substantially increased from 12% to 32% with the latter. The elaborated streaky flow excited in the boundary layer (e.g., with aforementioned MVGs) suffers from considerable viscous dissipation. To prevent the rapid decay of streaks, multiple MVGs in the streamwise direction could be necessary.[15] The control was also shown to be robust when subjected to random noise. On the other hand, some disadvantages are reported for MVG/roughness elements. (1) Under off-design flow conditions, the MVGs hardly play a positive role in maintaining

[a)]Electronic mail: jieren@tsinghua.edu.cn
[b)]Electronic mail: fs-dem@tsinghua.edu.cn
[c)]Also at Swedish Defence Research Agency (FOI), Stockholm, Sweden. Electronic mail: hanifi@kth.se

laminar flows; (2) when the flow is exposed to FST, this passive control could fail because of the interactions between the MVGs and FST. Recently, free-stream vortices are proved to be able to generate effective streaks.[19] This provides a new strategy through which the above weakness may be overcome.

Apart from the two-dimensional (2-D) disturbances in a flat-plate boundary layer, streaks can stabilize the oblique waves[11,20] as well. A similar approach for transition control in three-dimensional boundary-layer flow over swept-wings has been studied intensively by Saric *et al.*[21,22] Here, the sub-critical crossflow modes are excited by the micron-sized roughness elements, which through their nonlinear interactions with the mean flow weakened the critical crossflow mode as well as its secondary instabilities.[23]

Up to today, most of the existing studies performed on this topic are confined to incompressible flows. The present study thus aims at understanding the mechanism in high-speed boundary layer flows as well as exploiting this potential control methodology. First mode and second mode are both considered. The formulation and methodology are described in Sec. II. Results on the stabilization of first and second modes are presented and discussed in Sec. III. The present study is concluded in Sec. IV.

II. METHODOLOGY AND FRAMEWORK OF INSTABILITY ANALYSIS

A. Governing equations of the disturbances

In the framework of the stability analysis, the instantaneous flow field $q = (\rho, u, v, w, T)$ is considered as a superposition of the perturbation $\tilde{q}$ on the laminar base flow Q. For a 2-D boundary layer,

$$q(x, y, z, t) = Q(x, y) + \tilde{q}(x, y, z, t). \tag{1}$$

The base flow investigated is given by the self-similar solution to the compressible boundary layer. To derive the perturbation equations, we substitute (1) into the compressible Navier-Stokes (N-S) equations and subtract the equations for the mean flow. The resulted equations can be written in a well-identified and compact form[24]

$$\begin{aligned} \boldsymbol{\Gamma}\frac{\partial \tilde{q}}{\partial t} + \boldsymbol{A}\frac{\partial \tilde{q}}{\partial x} + \boldsymbol{B}\frac{\partial \tilde{q}}{\partial y} + \boldsymbol{C}\frac{\partial \tilde{q}}{\partial z} + \tilde{\boldsymbol{D}}q \;=\; & \boldsymbol{V}_{xx}\frac{\partial^2 \tilde{q}}{\partial x^2} + \boldsymbol{V}_{yy}\frac{\partial^2 \tilde{q}}{\partial y^2} + \boldsymbol{V}_{zz}\frac{\partial^2 \tilde{q}}{\partial z^2} + \boldsymbol{V}_{xy}\frac{\partial^2 \tilde{q}}{\partial x \partial y} \\ & + \boldsymbol{V}_{yz}\frac{\partial^2 \tilde{q}}{\partial y \partial z} + \boldsymbol{V}_{zx}\frac{\partial^2 \tilde{q}}{\partial z \partial x} + \tilde{\boldsymbol{N}}. \end{aligned} \tag{2}$$

The matrices $\boldsymbol{\Gamma}$, $\boldsymbol{A}$, $\boldsymbol{B}$, ... in (2) are functions of the mean flow quantities (detailed expressions can be found in the authors' previous papers[25]). Formulation of the nonlinear parabolized stability equations (NPSE) is standard and thus omitted here. Readers may refer to Herbert[26] for overview of the method, and Li and Malik[27] and Andersson *et al.*[28] for numerical issues related to the residue ellipticity of the equations.

In the present study, the space coordinates are scaled with the boundary layer length scale $\delta_0^* = \sqrt{\nu_\infty^* x_0^* / U_\infty^*}$ where asterisk stands for dimensional quantities. x_0 is the streamwise coordinate of a specified position. All the flow quantities are scaled with their free-stream values except the pressure by $\rho_\infty^*(U_\infty^*)^2$. The flow is thus characterized with the following dimensionless numbers:

$$Re_0 = \frac{\rho_\infty^* U_\infty^* \delta_0^*}{\mu_\infty^*},\; Ma = \frac{U_\infty^*}{\sqrt{\gamma R_{air}^* T_\infty^*}},\; Pr = \frac{\mu_\infty^* C_p^*}{\kappa_\infty^*}. \tag{3}$$

B. Perturbations in hypersonic boundary layers

In 2-D hypersonic boundary layers, Mack's second mode.[29] usually has the largest growth rate thus becoming the dominant instability. Employing the terminology suggested by Fedorov and Tumin,[30] this mode becomes unstable when the fast mode (mode F) and slow mode (mode

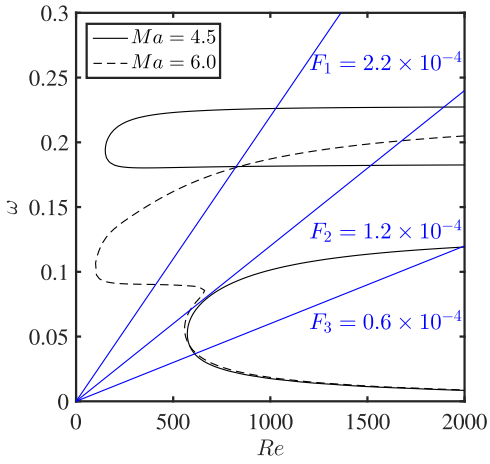

FIG. 1. Neutral curves of two-dimensional disturbances in hypersonic boundary layers with $Ma = 4.5$ and 6.0.

S) synchronize with each other.[31,32] Second mode can be mode F or mode S depending on the branching of the discrete spectrum.[33] In fact, the amplification of second mode is related to both mode F and mode S, i.e., a *double-mode* activity.

The neutral curves of the 2-D disturbance in Re–ω plane at $Ma = 4.5$ and 6.0 are shown in Fig. 1. $Re = \sqrt{\rho^*_\infty U^*_\infty x^*/\mu^*_\infty}$ is used as a measure of the streamwise coordinate. In the range of the parameters considered here, the unstable regions of first and second modes are well separated for $Ma = 4.5$ while they overlap at $Ma = 6.0$. The current study employs the perturbations with frequencies $F_1 = 2.2 \times 10^{-4}$, $F_2 = 1.2 \times 10^{-4}$, and $F_3 = 0.6 \times 10^{-4}$ where $F = \omega/Re$. The parameters of the four cases studied are listed in Table I. Perturbations considered in cases 1 and 2 are second- and first mode, respectively. Note that in the $Ma = 6.0$ flow (cases 3 and 4), perturbations with F_2 and F_3 manifest both first and second modes successively.

All the cases share the following parameters: stagnation temperature $T^*_s = 333$ K, Prandtl number $Pr = 0.7$, and Reynolds number $Re_0 = 300$. Adiabatic wall boundary condition is specified for the mean flow. If in a typical experimental configuration (see, for example, Fedorov *et al.*[34]), the stagnation pressure is specified to be $p^*_s = 10^5$ Pa, then the related dimensional flow quantities will correspond to those provided in Table II.

In Fig. 2, the evolution of the discrete spectrum at $Ma = 4.5$ and 6.0 for all the three frequencies are presented. At low Reynolds numbers, the mode S and mode F synchronize with the slow ($c_r = 1 - 1/Ma$) and fast acoustic waves ($c_r = 1 + 1/Ma$), respectively. Further downstream, the phase velocity of mode S increases and mode S may become unstable once passing through branch-I of the neutral curve of first mode. Accordingly, the phase velocity of mode F decreases. The synchronization between the mode F and the entropy/vorticity wave takes place when $c_r = 1$.[35] Finally, the synchronization between mode S and mode F starts when they have the same phase velocity. This process remains for a range of Re and is responsible for the growth of second mode as

TABLE I. The flow and disturbance parameters for 2-D perturbations studied in the current work.

Flow case	Flow parameters	Perturbations
Case 1	$Ma = 4.5,\ F = F_1$	Second mode[a]
Case 2	$Ma = 4.5,\ F = F_3$	First mode[b]
Case 3	$Ma = 6.0,\ F = F_2$	First and second mode[a]
Case 4	$Ma = 6.0,\ F = F_3$	First and second mode[a]

[a]Mode F/S
[b]Mode S

TABLE II. A set of typical dimensional flow parameters for experimental reproduction (subjected to $p_s^* = 10^5$ Pa).

Ma	T_∞^* (K)	p_∞^* (Pa)	U_∞^* (m/s)	ρ_∞^* (kg/m^3)	x_0^* (mm)
4.5	65.94	345.53	733.11	0.018	29.7
6.0	40.61	63.34	767.10	0.0054	53.9

well as the branching of the spectrum.[31] When curvature is present, the above synchronizations can be substantially influenced.[36]

C. The streaks

As introduced in Section I, the Görtler modes or Klebanoff modes are natural and straightforward streak generators. They both manifest as counter-rotating streamwise vortices[37] and give rise to boundary layer streaks through *lift-up* mechanism.[38–40] The primary differences between the two are as follows: (i) Görtler modes are non-modal in small Re regime and approach exponential modal growth when the Re is asymptotically large.[41] Whereas Klebanoff modes are fundamentally non-modal and can be recovered either with a linear combination of the eigenmodes or with the adjoint equations iteratively accounting for the non-parallel effects. (ii) The Görtler modes are driven by the centrifugal instability and can keep growing before entering the right branch regime.[41]

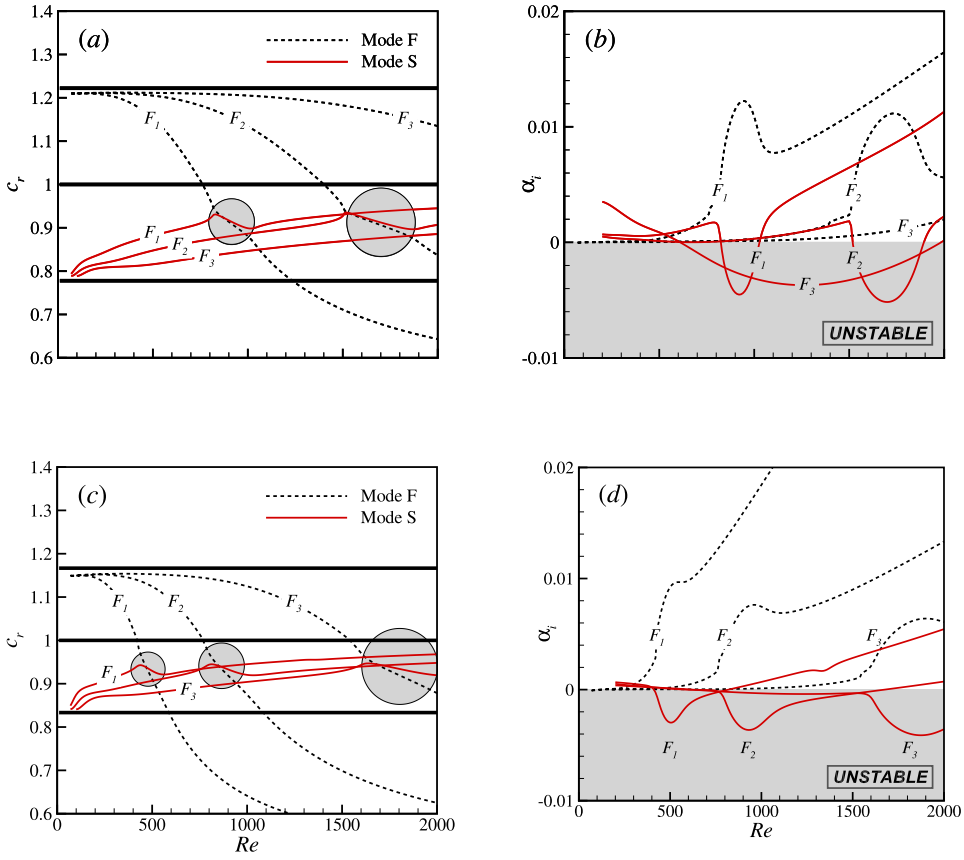

FIG. 2. Evolution of the discrete spectrum of perturbations with frequency F_1, F_2 and F_3. Phase velocity c_r and growth rate α_i are provided for $Ma = 4.5$ (a) and (b) and $Ma = 6.0$ (c) and (d), respectively. The regions of synchronization between mode F and mode S are circled in the diagram of the phase velocity. The thick straight line in (a) and (c) indicate the phase velocity of the fast acoustic wave ($c_r = 1 + 1/Ma$), entropy/vorticity wave ($c_r = 1$), and slow acoustic wave ($c_r = 1 - 1/Ma$), respectively. The growth rate $-\alpha_i$ of the mode S with $F = F_3$ at $Ma = 4.5$ is multiplied with 10 for a clear demonstration in (b).

On the other hand, the Klebanoff modes would be amplified in a rather limited range and therefore their growth is termed the *transient growth*.

The optimal disturbances can be computed using an eigenfunction expansion or a marching approach (with adjoint equations). In compressible boundary layers, they are described in work by Hanifi *et al.*[42] and Tumin and Reshotko.[43,44] The readers may refer to these papers for the formulation and relevant computational methods. Here, we utilize the local approach to compute the optimal perturbations. The energy norm used in this article follows the one defined by Mack[45] and Hanifi *et al.*,[42] i.e.,

$$\langle \tilde{\boldsymbol{q}}_1, \tilde{\boldsymbol{q}}_2 \rangle = \int_0^\infty \tilde{\boldsymbol{q}}_1^H \boldsymbol{M} \tilde{\boldsymbol{q}}_2 \, \mathrm{d}y, \tag{4}$$

with $\boldsymbol{M} = \mathrm{diag}\left(\frac{\tilde{T}}{\rho\gamma Ma^2}, \rho, \rho, \rho, \frac{\rho}{\gamma(\gamma-1)\tilde{T}Ma^2}\right)$ and $\tilde{\boldsymbol{q}} = \left(\tilde{\rho}, \tilde{u}, \tilde{v}, \tilde{w}, \tilde{T}\right)^T$. The norm eliminates pressure related energy transfer terms from the perturbation energy

$$\|\tilde{\boldsymbol{q}}\|_E = \frac{1}{2}\langle \tilde{\boldsymbol{q}}, \tilde{\boldsymbol{q}} \rangle . \tag{5}$$

The local linear stability equations are solved as an eigenvalue problem. The parallel base flow is assumed. Again, with standard procedures, the optimal disturbance is then given by a linear combination of the eigenvectors. The readers may refer to the article by Schmid and Brandt.[46]

Fig. 3 shows the maximum energy growth $G(x)$ versus the streamwise coordinate x. In the $Ma = 3.0$ case, shown in Fig. 3(a), the results are compared with Tumin and Reshotko.[43] The local

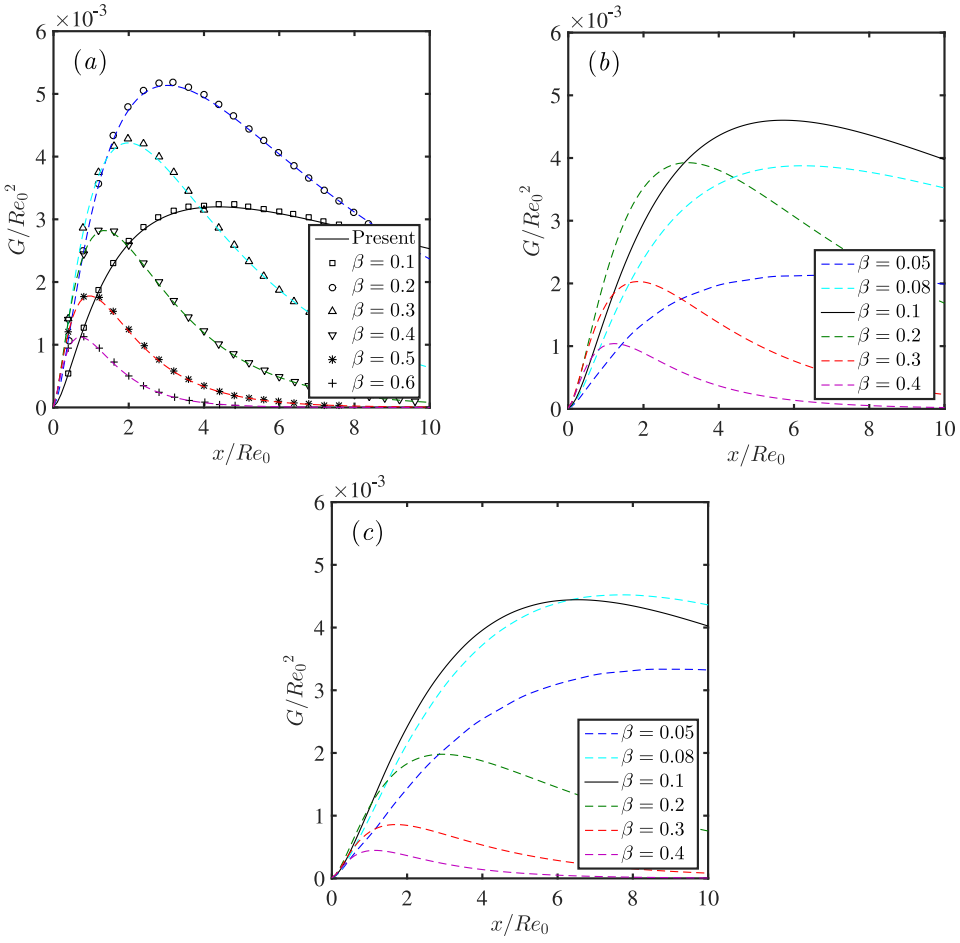

FIG. 3. Maximum energy growth $G(x)$ of the optimal disturbances. $Re_0 = 300$, $T_s^* = 333$ K. (a) $Ma = 3.0$, symbols denote results from Tumin and Reshotko,[43] (b) $Ma = 4.5$, and (c) $Ma = 6.0$.

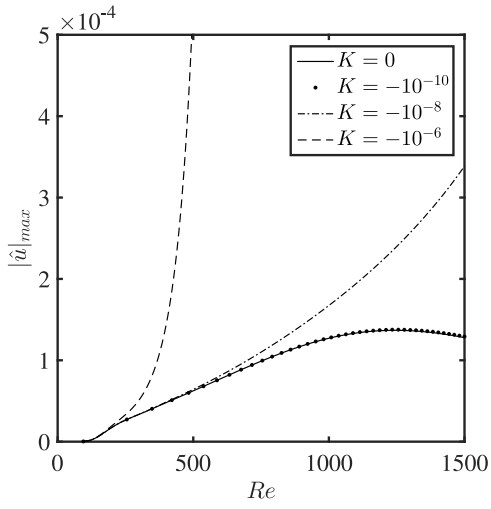

FIG. 4. Effect of concave curvature on the linear spatial development of streaks: from Klebanoff-type to Görtler-type. Maximum value of streamwise velocity component $|\hat{u}|_{max}$ is plotted as a function of Re. $T_s^* = 333$ K, $Ma = 4.5$.

boundary layer is given by a self-similar solution at $Re = Re_0 = 300$. Within the range of spanwise wavenumber considered here, $\beta = 0.2$ gives the largest energy growth G_{max}. This amplification ratio also depends on the streamwise coordinate of the inlet x_0 and outlet x_1. As shown in Figs. 3(b) and 3(c), increasing the Mach number to 4.5 and 6.0 causes the transient growth of perturbation with larger wavenumber (e.g., $\beta > 0.1$) to decrease and for those with smaller β to increase. The optimal wavenumber β_{opt} thus decreases. For the three Mach numbers considered here, streaks with $\beta = 0.1$ experience a sufficient transient growth. Therefore, they are employed in this study to stabilize the boundary layer.

When a large enough concave curvature is present, Görtler instability becomes the leading mechanism for the amplification of streaks as shown in Fig. 4. We define the global curvature K as $K = k/Re = -\nu_\infty^*/(U_\infty^* R^*)$ where R^* is the local radius of curvature and k is local curvature. A flat plate as well as concave plates (with three different curvatures) are compared. The spatial amplification of streaks attributes to the transient growth over a flat ($K = 0$) or very weakly curved ($K = -10^{-10}$, for example) plate. This is finally replaced with exponential growth for larger curvatures ($K = -10^{-8}$ and -10^{-6}). The influence of curvature on the streak profiles is shown in Fig. 5. Normalized streamwise velocity profiles $|\hat{u}|$ contributed by streaks are plotted uniformly distributed within $477 \le Re \le 1498$. By increasing the curvature, differences become evident further downstream where the Görtler modes tend to get closer to the wall than Klebanoff modes. It should be

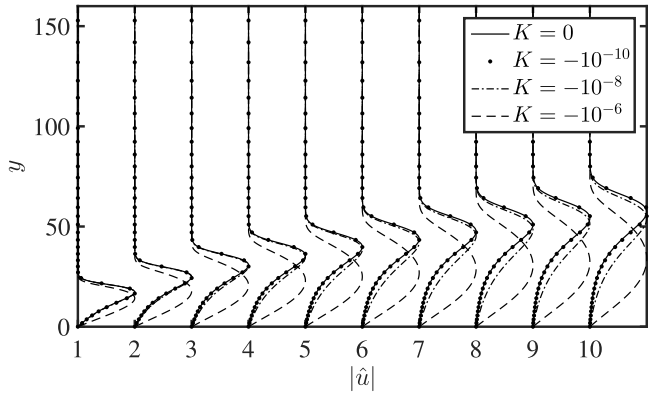

FIG. 5. Profiles of the streamwise velocity component $|\hat{u}|$ distributed within $477 \le Re \le 1498$. They are normalized to have unit maximum value. $T_s^* = 333$ K, $Ma = 4.5$.

noted that, a continuous transformation from Klebanoff modes to Görtler modes can be achieved by gradually increasing the curvature. To investigate these two type of modes, in the present paper we study streaks in cases with $K = 0$ and $K = -10^{-6}$. These are termed here Klebanoff-type (K-type) and Görtler-type (G-type) streaks, respectively.

The steady Görtler or Klebanoff mode with spanwise wavenumber $\beta = 0.1$ is introduced into the laminar boundary layer either near the leading edge $Re < 100$ (for Klebanoff mode) or at $Re = Re_0 = 300$ (for Görtler mode). The 2-D disturbances are obtained from the local eigenmode and they are added to the flow at $Re = 500$ (ahead of branch-I of the neutral curve). The Klebanoff mode has been optimized for $Re = 1200$ with the inlet corresponding to $Re = Re_0 = 300$.

III. RESULTS AND DISCUSSIONS

A. Interaction with Klebanoff-type streaks

The stabilizing effects on first and second modes are investigated first at $Ma = 4.5$. The modal perturbations of frequencies F_1 and F_3 become unstable as second- and first mode, respectively, as shown in Fig. 1. The interaction between the streak and first/second mode is computed through the following procedure. The Klebanoff mode (mode$(0,\pm1)$) is introduced into the boundary layer near the leading edge. Initially this perturbation is integrated linearly up to a given position eliminating the influence of initial transient behavior. The amplitude of the Klebanoff mode is then prescribed and nonlinear development of the streak is followed downstream. The 2-D disturbance (mode$(1,0)$) is later initialized at $Re = 500$ with a sufficient low amplitude thus ensuring linearity. The number of Fourier components kept in the calculation is -12 to 12 in the spanwise wavenumber and 0 to 3 in the frequency which has been tested to be sufficient to characterize the nonlinear interactions.

Four sets of streaks of different amplitudes are denoted as $K1$, $K2$, $K3$, and $K4$. The spatial development of the streaks as a function of the local Reynolds number Re is presented in Fig. 6. The maximum amplitudes are $A(u) = 1.1\%$, 2.2%, 3.4%, and 4.7%, respectively. The amplitude is defined as

$$A(u) = 0.5\left(\max_{y,z}(\tilde{u}) - \min_{y,z}(\tilde{u})\right) \tag{6}$$

The amplitude of the T-S waves measured in terms of temperature and streamwise velocity perturbations are given in Fig. 7. The temperature perturbation T' has the largest amplitude in hypersonic flows considered here and can be regarded as a measure of $|q'|_{max}$. The dashed lines

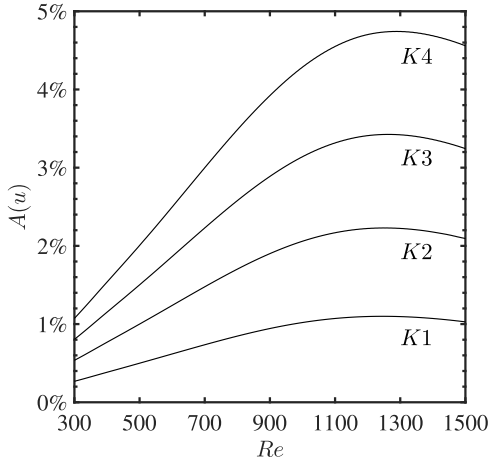

FIG. 6. Spatial development of the streak amplitude. The maximum amplitudes are $A(u;K1) = 1.1\%$, $A(u;K2) = 2.2\%$, $A(u;K3) = 3.4\%$, and $A(u;K4) = 4.7\%$, respectively.

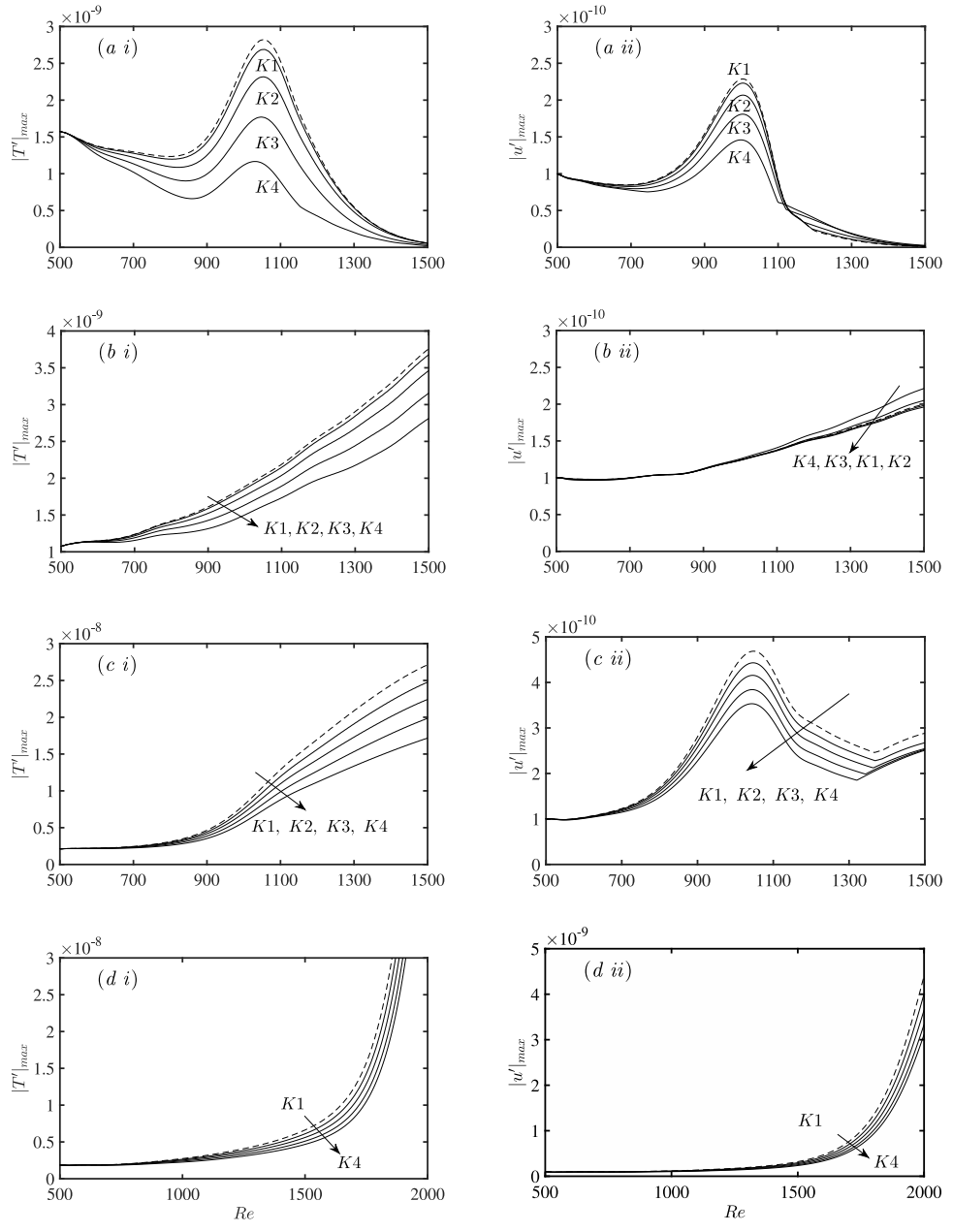

FIG. 7. Evolution of the 2-D perturbations in a streaky (Klebanoff-type) flow with $Ma = 4.5$ and $Ma = 6.0$. The initial amplitude of the 2-D perturbation is $|u'|_{max} = 10^{-10}$. The amplitude of the temperature and streamwise velocity perturbations $|T'|_{max}$ and $|u'|_{max}$ is shown here. $K1$, $K2$, $K3$, and $K4$ indicate the streaks of different amplitudes. Development of the 2-D perturbations without streaks is shown with dashed lines. (a) Second mode (case 1, $F = F1$). (b) First mode (case 2, $F = F3$). (c) First/second mode (case 3, $F = F2$). (d) First/second mode (case 4, $F = F3$).

indicate the amplitude of the 2-D perturbations in the absence of streaks. It is therefore obvious that the streaks can stabilize both first and second modes. An increase of the streak amplitude resulted in a stronger stabilization. This is demonstrated as decreased amplitude of the 2-D perturbations in Figs. 7(a) and 7(b). It is worth noting that the effect of streaks on the component of u' is not always stabilizing, e.g., first mode shown in Fig. 7(b ii). Since $|u'|$ is one order of magnitude smaller than $|T'|$, the general stabilizing effect should not be influenced.

In hypersonic boundary layers, perturbations can be co-modulated by first and second modes, e.g., the $Ma = 6.0$ boundary layer (cases 3 and 4). Here, we consider perturbations with frequency

$F = F2$ and $F = F3$. With the increase of Re, they behave as first- and second mode successively. Second mode exerts relatively more influence on case 3 ($F = F2$). The streaks included here are of Klebanoff-type. The maximum amplitudes are $A(u) = 0.75\%(K1)$, $1.2\%(K2)$, $1.6\%(K3)$, and $2.1\%(K4)$ in case 3. In case 4, they are 0.71%, 1.1%, 1.5%, and 1.9%. The stabilization is revealed

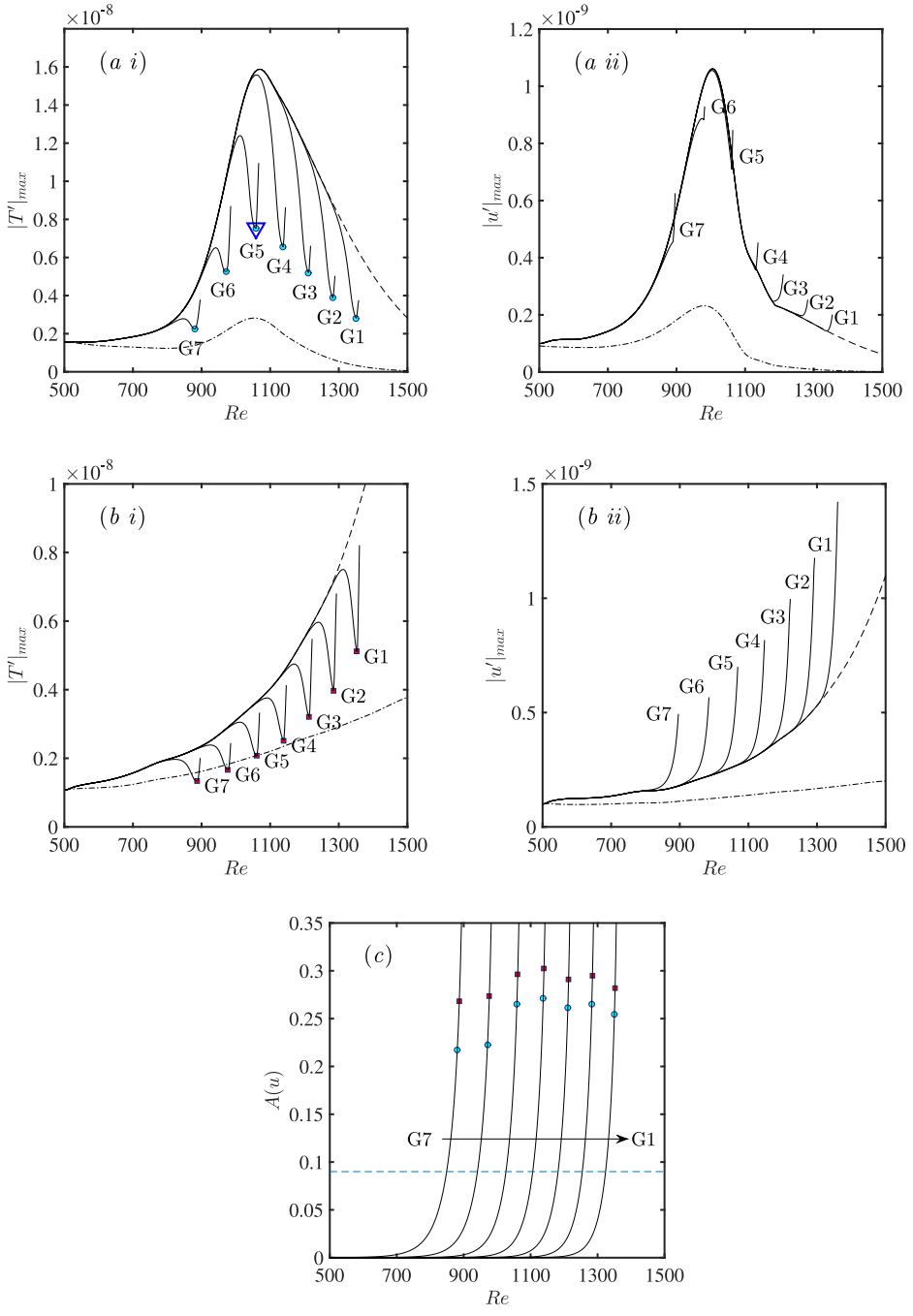

FIG. 8. Evolution of the 2-D perturbations in a streaky (Görtler-type) flow with $Ma = 4.5$. The initial amplitude of the 2-D perturbation is $|u'|_{max} = 10^{-10}$. The amplitude of the temperature and streamwise velocity perturbation $|T'|_{max}$ and $|u'|_{max}$ is shown here. $G1, G2, \ldots, G7$ indicate the streaks of different initial amplitudes. Development of the 2-D perturbations without streaks is shown with dashed lines. Dashed-dotted lines correspond to the result without curvature (same as the dashed lines in Figs. 7(a) and 7(b)). The circle and square symbols indicate the onset of secondary instability. The profiles for G5 near the onset of secondary instability (denoted with a triangle) are given in Figs. 9(c) and 9(d). (a) Second mode (case 1, $F = F1$). (b) First mode (case 2, $F = F3$). (c) Spatial development of the streaks.

in Figs. 7(c) and 7(d) indicating that the combined first/second mode can be effectively stabilized with finite amplitude streaks as well.

B. Interaction with Görtler-type streaks

When concave curvature is present, Görtler instability can play a dominant role. On concave walls, first/second modes become more unstable as well (see also Ref. 36). The streamwise curvature ($K = -10^{-6}$) included here stands for the most commonly investigated case and represents typical Görtler instability (see Sec. II). Fig. 8 shows the interactions between Görtler instability and first/second mode. The dashed-dotted lines (without curvature) and dashed lines (with curvature) in Figs. 8(a) and 8(b) indicate the flow without streaks. Both first and second modes are enhanced by concave curvature. Görtler vortices with different amplitudes are considered($G1,\ G2, \ldots,\ G7$). The initial amplitudes are prescribed as $A(u; G1) = 2 \times 10^{-11}$, $A(u; G2) = 2 \times 10^{-10}, \ldots, A(u; G7) = 2 \times 10^{-5}$. In the current Görtler flow, the threshold amplitude[47] for the sinuous secondary instability is close to $A(u) = 9\%$ and is shown with a dashed line in Fig. 8(c). The streak amplitude increases rather fast and exceeds this critical value regardless of the initial amplitude. Figs. 8(a) and 8(b) shows the evolution of second/first mode in the presence of Görtler-type streaks. The perturbations

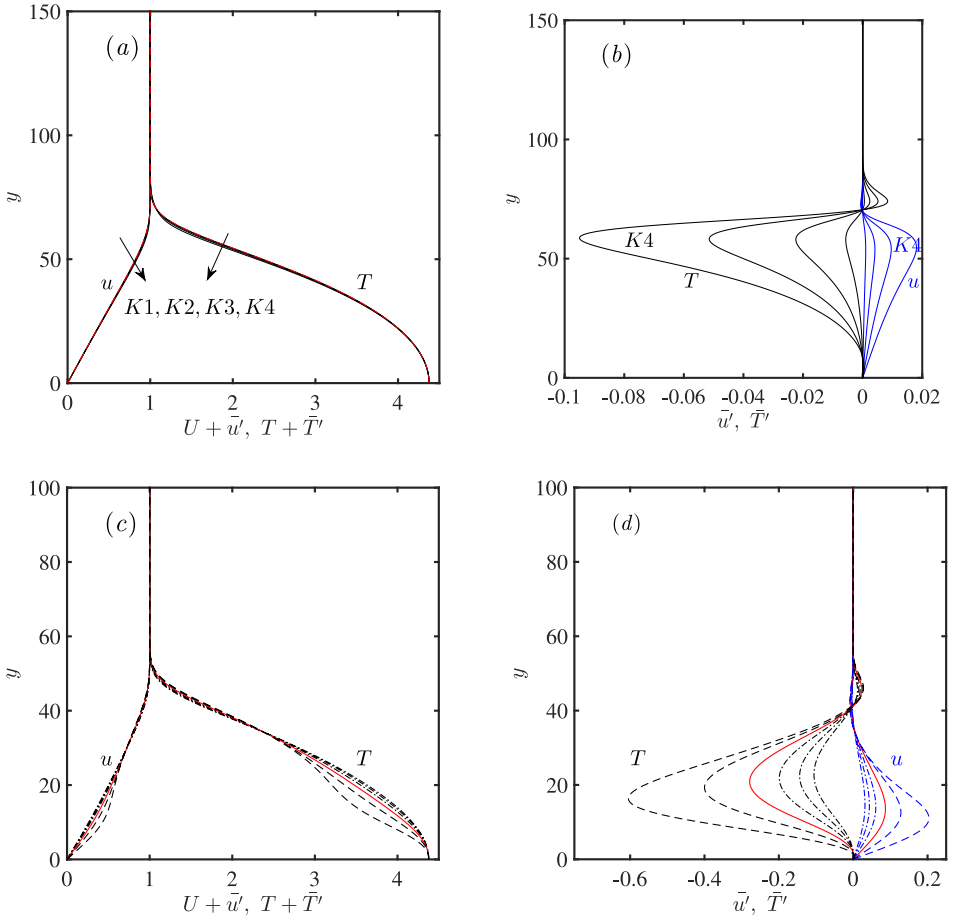

FIG. 9. Spanwise averaged total (a) and (c) and perturbation (b) and (d) velocity and temperature profiles at $Ma = 4.5$ (cases 1 and 2). Klebanoff-type streaks are shown at $Re = 1500$ in (a) and (b). The red dashed lines correspond to the boundary layer without streaks. Görtler-type streaks are shown in (c) and (d) with an initial amplitude of $A(u) = 2 \times 10^{-7}$ (G7). The red solid lines indicate the profile at $Re = 1059$ according to the triangle symbol (onset of secondary instability) in Fig. 8(a). Inflection points arise from this position and become more obvious downstream (see dashed lines at $Re = 1064$ and 1069). Dashed-dotted lines in (c) and (d) shows the profiles at $Re = 1044,\ 1049$, and 1054 which are before the onset of secondary instability.

though, can be stabilized by a certain extent, they finally become more unstable due to the secondary instability of the streaks. This is shown with a sudden uplift of the amplitude. The circle and square symbols indicate the uplift point of $|T'|_{max}$. As can be found in Sec. III C, it is the secondary instability of streaks that causes the failure of stabilization. Calculations are stopped before the amplitude becomes extremely large and computations blow up.

C. Mechanisms of stabilization

In hypersonic boundary layers, both first and second modes (as well as combined first/second mode) can be effectively stabilized by finite amplitude streaks. The key mechanism behind lies in the modification of the base flow by the nonlinear interaction with streaks. Fig. 9 shows the spanwise averaged total (a,c) and perturbation (b,d) velocity and temperature profiles at $Ma = 4.5$. The Klebanoff-type streaks at $Re = 1500$ are shown in Figs. 9(a) and 9(b). The base flow is modified into a fuller profile. This modification becomes more obvious when the streak amplitude is increased. In Figs. 9(c) and 9(d) similar data are presented for the Görtler-type streaks with the initial amplitude of $A(u) = 2 \times 10^{-7}$ (G5). The solid red lines indicate the profile at $Re = 1059$ which corresponds to the triangle symbol in Fig. 8(a). The dashed-dotted lines show the profiles at

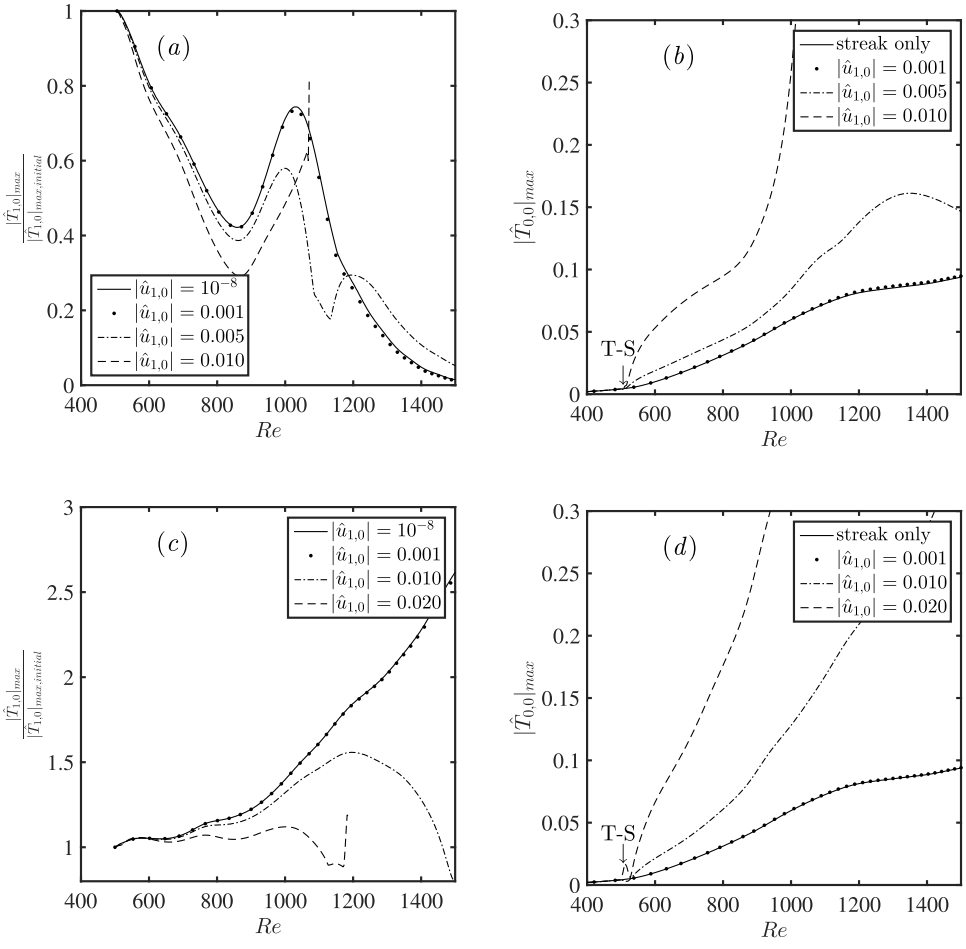

FIG. 10. Nonlinear development of 2-D perturbation in streaky flat-plate flows at $Ma = 4.5$. Streak amplitude corresponds to K4 with a maximum $A(u) = 4.7\%$. (a) Amplitude of second mode (case 1) measured with $|\hat{T}_{1,0}|_{max}$. The initial amplitude is prescribed as $|\hat{u}_{1,0}| = 10^{-8}$, 0.001, 0.005, and 0.01, respectively. The curves are scaled with the initial value at $Re = 500$. (b) Modification to the mean flow measured with $|\hat{T}_{0,0}|_{max}$ with the presence of streaks and second mode (case 1). (c) and (d) Same as (a) and (b) but for first mode (case 2). The initial amplitude is $|\hat{u}_{1,0}| = 10^{-8}$, 0.001, 0.01, and 0.02, respectively.

Re = 1054, 1049, and 1044 where the 2D perturbations are stabilized. The dashed lines show the profiles at Re = 1064 and 1069 where the flow becomes secondary unstable. It is obvious that both the velocity and temperature profiles become inflectional at Re = 1064 and 1069, giving rise to the secondary instability (inviscid in nature).

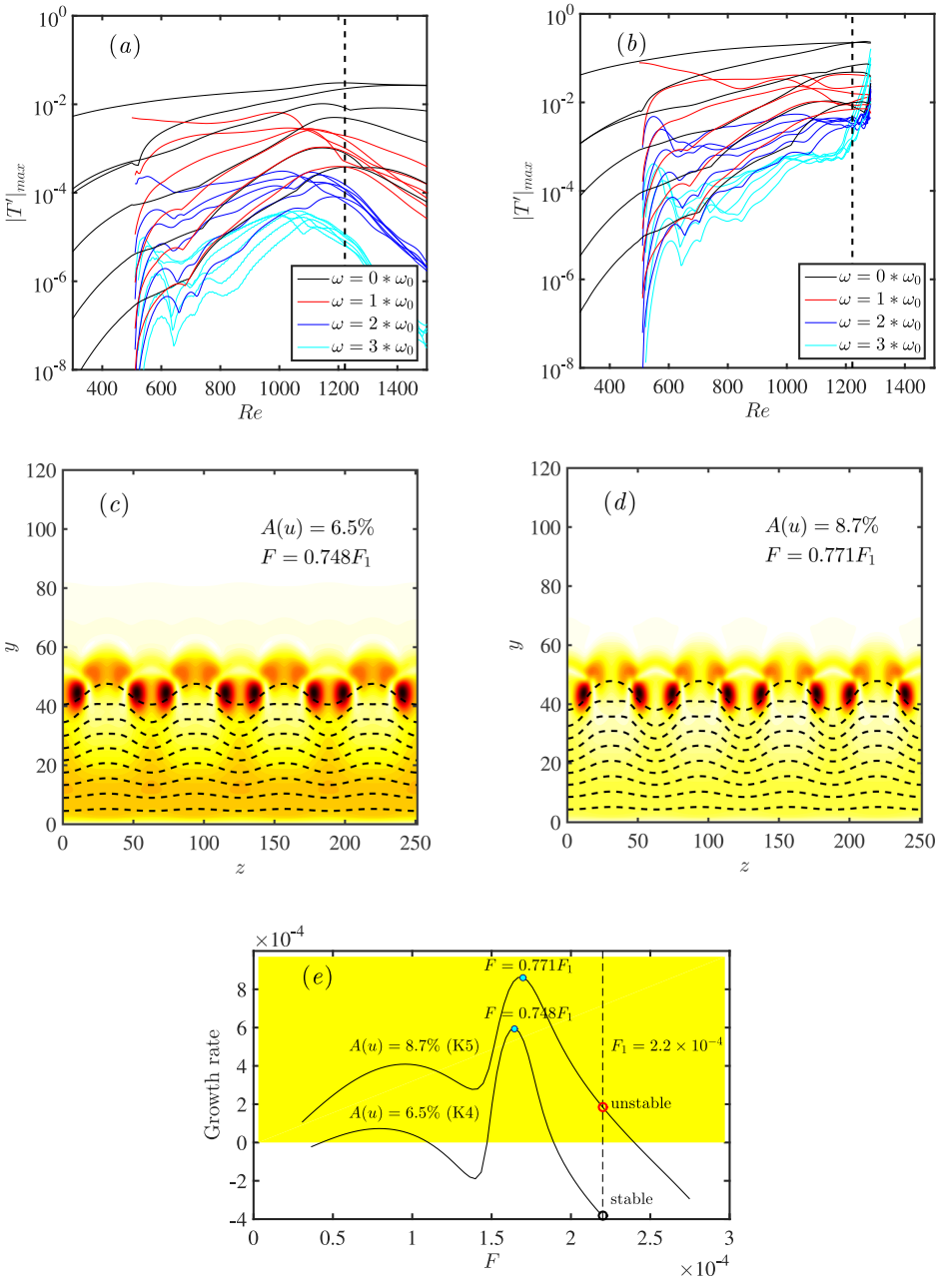

FIG. 11. (a) and (b) Nonlinear development of 2-D perturbation in streaky flat-plate flows at $Ma = 4.5$. Amplitude of the mode (m,n) with $m = 0,\ 1,\ 2,\ 3$ and $n = 0,\ 1,\ 2, \ldots, 5$. $F = F_1$ (second mode). Initial amplitude of 2-D perturbation $|\hat{u}_{1,0}| = 0.005$. The dashed lines show the position at $Re = 1222$ where secondary instability analysis is performed. Initial streak amplitude corresponds to K4 (a) and K5 (b). (c) and (d) Secondary instability of the time-averaged streaky flows (four periods shown in spanwise). Contour lines show the streamwise velocity of the base flow. Nine equally spaced contour levels are from 0.1 to 0.9. The corresponding secondary perturbations (of the most unstable frequency) are shown with colored contours. (e) Growth rate of the secondary perturbation as a function of the dimensionless frequency F. The colored area shows the unstable half-plane. The solid (blue) circles indicate the most unstable frequency. The dashed line shows the frequency $F_1 = 2.2 \times 10^{-4}$ of the 2-D perturbation.

D. Nonlinear effects

In the study above, we have considered 2-D perturbations of small amplitudes. When their amplitudes are increased, e.g., to the same order of streaks, fully nonlinear interactions both in the spanwise wavenumber and frequency spaces can result in a multi-fold influence on the perturbations.

To examine the interaction of streaks with the nonlinear 2-D perturbations, calculations are performed for four different amplitudes of these waves. Here, the initial amplitude of streaks is the same as K4 ($A(u)_{max} = 4.7\%$) in Sec. III. The results are presented in Fig. 10. The infinitesimal amplitude $|\hat{u}(1,0)|_{max} = 10^{-8}$ represents the linear case. In nonlinear cases, the exponential growth of mode $(1,0)$ (the perturbation of main interest) is damped due to redistribution of energy to its super-harmonics. A stronger stabilization effect is thus shown in Figs. 10(a) and 10(c) both for first and second modes. Comparison with the *linear* case shows that the nonlinear interactions become noticeable when the initial amplitude is rather large, e.g., $\hat{u}_{1,0} > 0.001$.

It is obvious here the most important interaction is between modes $(0,1)$ and $(0,-1)$ in current streaky flows. In the fully nonlinear cases interaction of modes $(1,0)$ and $(-1,0)$ becomes dominating as well. Both interactions give rise to mode $(0,0)$ modifying the mean flow. Figs. 10(b) and 10(d) shows a larger amplitude of mode $(0,0)$ with increasing the amplitude of mode $(1,0)$. The mean flow is modified to a larger degree as a result. The secondary instability will have a chance to set-in, e.g., in Figs. 10(a) and 10(c) where $|\hat{u}_{1,0}| = 0.01$ and 0.02, respectively. Therefore, it should be underlined that this passive control may fail with a too large amplitude of either streaks or 2-D perturbations.

Here, we investigate the mechanism on the failure of stabilization in a fully nonlinear framework. The fundamental 2-D wave has an initial amplitude of $|\hat{u}_{1,0}| = 0.005$ and the initial amplitudes of streaks correspond to K4 ($A(u)_{max} = 4.7\%$) and $A(u)_{max} = 6.0\%$ (termed K5), respectively. Both amplitudes $A(u)_{max}$ are measured with infinitesimal 2-D perturbation. The actual amplitudes are thus larger. The results are shown in Fig. 11 where the amplitude of modes with $m = 0,\ldots,3$ and $n = 0,\ldots,5$ are plotted. In the case of with K4 streak, the perturbations can still be successfully stabilized as shown in Fig. 11(a) where fully nonlinear interactions are present. With stronger streaks in Fig. 11(b), though modes $(1,n)$ can be suppressed at some point, they finally become unstable along with their super-harmonics (e.g., modes $(2,n)$ and $(3,n)$) and get amplified rather quickly. A secondary instability analysis is thus given for the time-averaged mean flow at $Re = 1222$ (see dashed lines in Figs. 11(a) and 11(b)). Secondary perturbations of streamwise velocity together with the mean flow are shown in Figs. 11(c) and 11(d) for the two cases. The frequency correspond to the most unstable point in Fig. 11(e). The streak amplitudes at this position are 6.5% and 8.7%, respectively. It is obvious that the secondary perturbation become unstable in both cases. They are of sinuous type and have a lower frequency compared to the 2-D perturbation. It is important to note the differences: (i) the growth rate of secondary perturbation with larger amplitude of streak is certainly larger. (ii) The unstable band of frequency in Fig. 11(c) is outside the 2-D perturbation while in (d) a larger band covers this frequency. This is responsible for the failure of stabilization in (b).

IV. CONCLUSION

From the above analysis, it can be concluded that the mechanism behind the stabilization in hypersonic boundary-layer flows is similar to that in incompressible flows — a favorable modification to the mean flow. Although the two modes are different in nature, this study shows that both first and second modes can be effectively stabilized with finite amplitude streaks. Klebanoff-type streaks are more interesting as they have a mild spatial growth and their amplitude is more controllable. With regard to the Görtler-type streaks, where curvature is large enough, the secondary instability becomes more inevitable due to exponential growth. The concave curvature, *per se*, destabilizes the perturbations. On the other hand, curvature can be regarded as an effective controller on streak amplitude offering further potential improvement and optimization of the control methodology.

ACKNOWLEDGMENTS

J. Ren and S. Fu acknowledge the financial support by the National Natural Science Foundation of China (Grant Nos. 11272183, 11572176, and 11572177), the National Key Basic Research Program of China (Grant No. 2014CB744801), and China Scholarship Council (No. 201406210236).

[1] K.-S. Choi, "Fluid dynamics: The rough with the smooth," Nature **440**, 754 (2006).
[2] S. J. Leib, D. W. Wundrow, and M. E. Goldstein, "Effect of free-stream turbulence and other vortical disturbances on a laminar boundary layer," J. Fluid Mech. **380**, 169–203 (1999).
[3] W. S. Saric, "Görtler vortices," Annu. Rev. Fluid Mech. **26**, 379–409 (1994).
[4] N. De Tullio, P. Paredes, N. D. Sandham, and V. Theofilis, "Laminar-turbulent transition induced by a discrete roughness element in a supersonic boundary layer," J. Fluid Mech. **735**, 613–646 (2013).
[5] P. Andersson, L. Brandt, A. Bottaro, and D. S. Henningson, "On the breakdown of boundary layer streaks," J. Fluid Mech. **428**, 29–60 (2001).
[6] C. Cossu, L. Brandt, S. Bagheri, and D. S. Henningson, "Secondary threshold amplitudes for sinuous streak breakdown," Phys. Fluids **23**, 074103 (2011).
[7] C. Cossu and L. Brandt, "Stabilization of Tollmien-Schlichting waves by finite amplitude optimal streaks in the blasius boundary layer," Phys. Fluids **14**, L57–L60 (2002).
[8] C. Cossu and L. Brandt, "On Tollmien-Schlichting-like waves in streaky boundary layers," Eur. J. Mech., B: Fluids **23**, 815–833 (2004).
[9] P. Andersson, M. Berggren, and D. S. Henningson, "Optimal disturbances and bypass transition in boundary layers," Phys. Fluids **11**, 134–150 (1999).
[10] P. Luchini, "Reynolds-number-independent instability of the boundary layer over a flat surface: Optimal perturbations," J. Fluid Mech. **404**, 289–309 (2000).
[11] S. Bagheri and A. Hanifi, "The stabilizing effect of streaks on Tollmien-Schlichting and oblique waves: A parametric study," Phys. Fluids **19**, 078103 (2007).
[12] J. H. M. Fransson, L. Brandt, A. Talamelli, and C. Cossu, "Experimental and theoretical investigation of the nonmodal growth of steady streaks in a flat plate boundary layer," Phys. Fluids **16**, 3627–3638 (2004).
[13] J. H. M. Fransson, L. Brandt, A. Talamelli, and C. Cossu, "Experimental study of the stabilization of Tollmien-Schlichting waves by finite amplitude streaks," Phys. Fluids **17**, 054110 (2005).
[14] J. H. M. Fransson, A. Talamelli, L. Brandt, and C. Cossu, "Delaying transition to turbulence by a passive mechanism," Phys. Rev. Lett. **96**, 064501 (2006).
[15] J. H. M. Fransson and A. Talamelli, "On the generation of steady streamwise streaks in flat-plate boundary layers," J. Fluid Mech. **698**, 211–234 (2012).
[16] S. Shahinfar, S. S. Sattarzadeh, J. H. M. Fransson, and A. Talamelli, "Revival of classical vortex generators now for transition delay," Phys. Rev. Lett. **109**, 074501 (2012).
[17] S. Shahinfar, J. H. M. Fransson, S. S. Sattarzadeh, and A. Talamelli, "Scaling of streamwise boundary layer streaks and their ability to reduce skin-friction drag," J. Fluid Mech. **733**, 1–32 (2013).
[18] S. S. Sattarzadeh and J. H. Fransson, "On the scaling of streamwise streaks and their efficiency to attenuate Tollmien-Schlichting waves," Exp. Fluids **56**, 58 (2015).
[19] L. Siconolfi, S. Camarri, and J. H. M. Fransson, "Boundary layer stabilization using free-stream vortices," J. Fluid Mech. **764**, R2 (2015).
[20] S. Shahinfar, S. S. Sattarzadeh, and J. H. M. Fransson, "Passive boundary layer control of oblique disturbances by finite-amplitude streaks," J. Fluid Mech. **749**, 1–36 (2014).
[21] W. S. Saric, R. B. Carillo, and M. S. Reibert, "Leading-edge roughness as a transition control mechanism," AIAA Paper No. 98-0781, 1998.
[22] W. S. Saric and H. L. Reed, "Supersonic laminar flow control on swept wings using distributed roughness," AIAA Paper 2002-0147, 2002.
[23] S. M. Hosseini, D. Tempelmann, A. Hanifi, and D. S. Henningson, "Stabilization of a swept-wing boundary layer by distributed roughness elements," J. Fluid Mech. **718**, R1 (2013).
[24] C.-L. Chang and M. R. Malik, "Oblique-mode breakdown and secondary instability in supersonic boundary layers," J. Fluid Mech. **273**, 323–360 (1994).
[25] J. Ren and S. Fu, "Competition of the multiple Görtler modes in hypersonic boundary layer flows," Sci. China: Phys., Mech. Astron. **57**, 1178–1193 (2014).
[26] T. Herbert, "Parabolized stability equations," Annu. Rev. Fluid Mech. **29**, 245–283 (1997).
[27] F. Li and M. R. Malik, "On the nature of PSE approximation," Theor. Comput. Fluid Dyn. **8**, 253–273 (1996).
[28] P. Andersson, D. Henningson, and A. Hanifi, "On a stabilization procedure for the parabolic stability equations," J. Eng. Math. **33**, 311–332 (1998).
[29] L. M. Mack, AGARD Report 709, Special Course on Stability and Transition of Laminar Flows, 1984.
[30] A. Federov and A. Tumin, "High-speed boundary-layer instability: Old terminology and a new framework," AIAA J. **49**, 1647–1657 (2011).
[31] A. Fedorov, "Transition and stability of high-speed boundary layers," Annu. Rev. Fluid Mech. **43**, 79–95 (2011).
[32] X. Zhong and X. Wang, "Direct numerical simulation on the receptivity, instability, and transition of hypersonic boundary layers," Annu. Rev. Fluid Mech. **44**, 527–561 (2012).
[33] V. Gushchin and A. Fedorov, "Excitation and development of unstable disturbances in a supersonic boundary layer," Fluid Dyn. **25**, 344–352 (1990).
[34] A. Fedorov, V. Soudakov, I. Egorov, A. Sidorenko, Y. Gromyko, D. Bountin, P. Polivanov, and A. Maslov, "High-speed boundary-layer stability on a cone with localized wall heating or cooling," AIAA J. **53**, 2512–2524 (2015).

[35] A. V. Fedorov and A. P. Khokhlov, "Prehistory of instability in a hypersonic boundary layer," Theor. Comput. Fluid Dyn. **14**, 359–375 (2001).
[36] J. Ren and S. Fu, "Study of the discrete spectrum in a Mach 4.5 Görtler flow," Flow, Turbul. Combust. **94**, 339–357 (2015).
[37] C. Cossu, J.-M. Chomaz, P. Huerre, and M. Costa, "Maximum spatial growth of Götler vortices," Flow, Turbul. Combust. **65**, 369–392 (2000).
[38] M. T. Landahl, "Wave breakdown and turbulence," SIAM J. Appl. Math. **28**, 735–756 (1975).
[39] T. Ellingsen and E. Palm, "Stability of linear flow," Phys. Fluids (1958-1988) **18**, 487–488 (1975).
[40] L. S. Hultgren and L. H. Gustavsson, "Algebraic growth of disturbances in a laminar boundary layer," Phys. Fluids (1958-1988) **24**, 1000–1004 (1981).
[41] P. Hall, "The linear development of Görtler vortices in growing boundary layers," J. Fluid Mech. **130**, 41–58 (1983).
[42] A. Hanifi, P. J. Schmid, and D. S. Henningson, "Transient growth in compressible boundary layer flow," Phys. Fluids **8**, 826–837 (1996).
[43] A. Tumin and E. Reshotko, "Spatial theory of optimal disturbances in boundary layers," Phys. Fluids **13**, 2097–2104 (2001).
[44] A. Tumin and E. Reshotko, "Optimal disturbances in compressible boundary layers," AIAA J. **41**, 2357–2363 (2003).
[45] L. M. Mack, Jet Propulsion Laboratory, California Institute of Technology, Pasadena, CA, USA, 1969.
[46] P. J. Schmid and L. Brandt, "Analysis of fluid systems: Stability, receptivity, sensitivitylecture notes from the FLOW-NORDITA summer school on advanced instability methods for complex flows, Stockholm, Sweden, 2013," Appl. Mech. Rev. **66**, 024803 (2014).
[47] J. Ren and S. Fu, "Secondary instabilities of Götler vortices in high-speed boundary layer flows," J. Fluid Mech. **781**, 388–421 (2015).